Steric effects on the rheology of nanocomposite gels of organoclay in dicarboxyl-terminated polybutadiene

Fei Li,[a] Katie Lania,[a] Xiaoliang Wang,[b] Gi Xue[b] and H. Henning Winter*[ac]

Received 19th October 2009, Accepted 30th March 2010
First published as an Advance Article on the web 28th April 2010
DOI: 10.1039/b921774f

Nanocomposite gels were formed by mixing organically modified clay into a linear, end-functionalized polymer (dicarboxyl-terminated polybutadiene). Two differently sized but otherwise similar counterions were chosen for preparing the organoclay. Hydrogen bonding between polymer and clay causes the polymer/clay interface to grow by splitting the clay aggregates into smaller clay particles, then swelling these particles, exfoliating the clay sheets, and eventually assuming a stable dispersion in the polymer matrix. The clay with the larger counterion exfoliates faster, but does not form the stronger network (lower modulus, lower yield stress), and it needs more clay to reach its gel point (percolation threshold ϕ_c). These seemingly contradictory observations (fast exfoliation but weak gel and later gel point) are attributed to steric effects of the larger macro-counterion. Parameters of the study are clay concentration ϕ and distance from the gel point. The low frequency linear viscoelastic behavior was analyzed using a percolation model (near ϕ_c) and a power law in concentration (far above ϕ_c). The use of two different organoclays allows comparison of the observed phenomena. The extent of agreement between experimental data and known models was used to theorize that the particle–polymer interactions are the controlling factor in the increasing solid-like behavior with increasing clay content.

1. Introduction

Properties of polymer/clay nanocomposites range from the very soft to the very hard. The combination of large surface area, high particle aspect ratio, strong particle–particle and/or particle–polymer interaction, in combination with nanoscale effects renders polymer–clay nanocomposites with superior thermal stability, gas/water barrier, and mechanical and optical properties which are not associated with pristine polymers and/or conventional filler/polymer materials.[1–10] This study is concerned with very soft physical gels that form a sample-spanning clay/polymer network structure which can be tuned by steric effects of macro-counterions on the clay surface. The study expands the work of Sun and coworkers[11–15] who have developed a new class of low molecular weight telechelic polymer/organoclay nanocomposites by simply compounding hydroxyl-terminated polybutadiene (HTPB) or carboxyl-terminated polybutadiene (CTPB) with montmorillonite clay that was organically modified with a cationic surfactant. For a clay concentration of up to 10 wt%, the exfoliation of such clay/polymer systems does not require mechanical energy input.

Zhu *et al.*[13] demonstrated that the number of alkyl tails of organic modifier is crucial for achieving a high degree of clay exfoliation at clay loadings up to 10 wt%. The single alkyl tail modified organoclay in CTPB requires heating above 80 °C to effectively overcome an energy barrier to exfoliation while the clay, which was treated with a counterion with two alkyl tails, exfoliates at 26 °C already. Time-resolved rheometry showed the growth of the gel modulus and the decay of the characteristic relaxation time during structural ripening of such a nanocomposite gel,[15,16] consisting of CTPB and organoclay containing one alkyl tail.

Montmorillonite as used in the above model system is a prime example of a layered silicate (clay) for preparing nanocomposites. The hydrophilic montmorillonite requires special conditioning to enhance its affinity with a hydrophobic (in most applications) polymer matrix. Surfactants, such as aliphatic amines or alkylphosphonium, commonly serve as organic modifiers to lower the clay surface energy to make it more compatible with the polymer. This furthers the diffusion of polymer chains into the clay galleries thereby expanding the interlayer spacing. This process is called intercalation. Eventually, clay particles exfoliate, *i.e.* they brake up into silicate sheets which randomly disperse throughout the nanocomposite. Exfoliation is preferred to intercalation since it maximizes physical properties. Exfoliation may be achieved in many different ways such as *in situ* intercalative polymerization,[17–20] emulsion polymerization,[21,22] sol–gel template synthesis,[23–25] and melt compounding.[26–30] Uniform dispersion often requires the aid of mechanical or thermal energy input as provided through single/twin screw extruders, shear mixers, or ultrasonicators. Optimum nanocomposite end-use performance was sought through suitable processing parameters (temperature, pressure, residence time, shear intensity) and/or composition variations (polymer matrix, polymer molecular weight, chemistry of organic modifier, compatibilizer).[26,27,29,31]

Small angle X-ray diffraction (SAXD) and transmission electron microscopy (TEM) are two sensitive techniques for

[a]*Dpt. Chemical Engineering, University of Massachusetts, Amherst, USA. E-mail: winter@ecs.umass.edu*
[b]*Dpt. Polymer Science and Engineering, Nanjing University, Nanjing, 210093, China*
[c]*Dpt. of Polymer Science and Engineering, University of Massachusetts, Amherst, USA*

characterizing the microstructure of polymer/clay nanocomposites. Rheology, first as a complementary measurement, has proven to be an advantageous tool for assessing the evolving dispersion states of silicates,[32] the role of particle–particle and particle–polymer interaction,[33–35] and sol–gel transition.[36–38] Most of these studies focus on properties of the final structure.

In this study, a UMass–UNanjing collaboration, we investigated the dependence of organoclay/CTPB rheology on counterion size and clay content. Two types of macro-counterions of similar composition but different size were used for comparison. The main parameters of this study are the ripening time, the modulus, and the critical strain. Observed trends and rheological data were fitted to the empirical and fundamental models for the intermolecular behavior of a nanocomposite.

2. Experiment

Material

The "sticky" end-functionalized polymer is a dicarboxyl-terminated 1,4-polybutadiene oligomer (CTPB) with M_n = 4200 (Aldrich Chemical). The CTPB was stabilized to prevent the degradation during rheological experiments at elevated temperatures.[39] CTPB is a fluid at room temperature which is advantageous for performing the ripening experiments (no solvent needs to be added). The two types of organically modified montmorillonite clay, purchased from Fenghong Clay Corp. (China), are denoted as DK1 and DK4. The organic modifier of DK1, the counterion octadecyltrimethylammonium (C18A) chloride, has a single alkyl tail in comparison to the two alkyl tails of the organic modifier of DK4, dioctadecyldimethylammonium (D18A) chloride. The initial interlamellar spacing of the two clays is 2.3 nm and 3.8 nm, respectively. For preparing a small batch of the organoclay (C18–clay), 10.0 g of industrially purified pristine montmorillonite (cation exchange capacity of 1 mequiv g^{-1}) gets dispersed into 1000 mL of distilled water at 87 °C for cation exchange with 3.5 g (equal to 1 mequiv g^{-1}) of octadecyltrimethylammonium chloride for 12 h. Washing with distilled water, checking with a 0.1 N $AgNO_3$ solution for residual Cl^- ions, and drying at 87 °C for 12 h finalizes the process. The number density of counterions is determined by the charge density on the clay surface. Because of this, an equal number density for DK1 and DK4 is assumed. DK1 and DK4 were prepared with the same raw clay. The same cation exchange capability of the raw material means a similar modifier density. The mass coverage by the counterions therefore is proportional to the size of the counterion which is higher for DK4.

The organoclay/CTPB nanocomposites were prepared by gently and quickly mixing metered amounts of clay with CTPB in a disposable vial at ambient temperature (15–20 °C) as described by Zhu *et al.*[13] While maintaining quiescent conditions, the structure ripens into a stable clay dispersion (denoted as "SCD" in the following) as has been demonstrated previously.[11–15] The resulting nanocomposites are highly exfoliated for clay contents up to 10 wt%. An irreversible SCD was achieved by heating the freshly mixed samples in the rheometer at a heating rate of 2 K min^{-1} with an upper temperature in the range of 26–116 °C as parameter. For DK1/CTPB, the highly exfoliated SCD can only form when the ripening temperature is above a critical value (≥80 °C). This temperature protocol has proven to successfully accelerate the ripening and ensure the fully developed SCD.[12] The slow ramp rate not only allows abundant ripening time, but also avoids shear and/or quench-cracking of the structure.

The unique physical and chemical properties of such polymer/clay colloids depend on the dispersion state of the clay nanostructure and the polymer–clay interaction.[40–42] Much is known about such polymer/clay systems.[4,8,43,44] This is advantageous for using the nanocomposite as model system.

Rheometry

The rheological measurements were performed on a strain-controlled rheometer (ARES; TA Instruments Corp.) with a torque transducer that autoranges between the full-scale of 200 g cm^{-1} with a 0.02 g cm^{-1} resolution and 2000 g cm^{-1} with a 0.2 g cm^{-1} resolution. The 2000 g cm^{-1} full scale is needed for large strain amplitude when determining the critical strain of the linear viscoelastic behavior for the most viscous composites. Cone-and-plate geometry of 50 mm diameter and 0.04 rad cone angle was chosen to ensure a uniform shear profile throughout the samples. 50 mm diameter parallel plates were preferred for samples with high clay content that made gap setting difficult for the cone-and-plate geometry (sample thicknesses between 0.5 mm and 1.0 mm). Agreement between the parallel-plate and the cone-and-plate data was found within the acceptable tolerance for mechanical spectroscopy, suggesting that wall-slip artifacts are negligible. The strain amplitude γ of small amplitude oscillatory shear (SAOS) was adjusted in the range of 0.001–0.005 according to the clay content. As selection criterion, γ was kept within the linear viscoelasticity region while being large enough for obtaining reasonable signal intensities at the experimental frequencies (0.01–100 rad s^{-1}) and temperatures (26–116 °C). The ARES gap auto-adjust function served to compensate the thermal expansion of the rheometer fixtures so that the sample thickness stayed constant over the large temperature range.

3. Results

Rheology of structural ripening during first heating

The structural ripening process in a freshly mixed sample accelerates at elevated temperatures. This expresses itself in a strong growth of the dynamic moduli (see Fig. 1) due to the

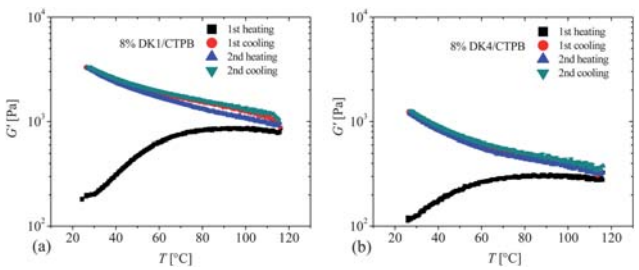

Fig. 1 Evolution of G' of 8 wt% clay/CTPB for DK1 (a) and DK4 (b) during structural ripening while ramping the temperature between 26 and 116 °C at 2 K min^{-1}. SAOS frequency: 1 rad s^{-1}. Heating and cooling are indicated in the legend.

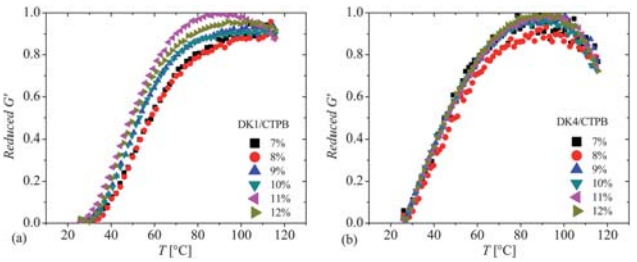

Fig. 2 Evolution of reduced G' of clay/CTPB for DK1 (a) and DK4 (b) in 1st heating cycle of the structural ripening. Temperature range: 26–116 °C; ramp rate: 2 K min^{-1}. SAOS frequency: 1 rad s^{-1}. Parameter is the clay content as indicated in the legend. At low clay content, the network connectivity is particularly weak, causing intensive noise in the rheological data, especially at early stages of ripening.

intercalation/exfoliation of the clay and the gradual formation of a three-dimensional network of clay sheets that is connected by attached polymer molecules (bridge molecules). Nearly all of the structuring occurs in the first heating. Subsequent heating and cooling cycles have little impact on G' (curves overlap), suggesting that the sample practically reaches its final, stable clay dispersion structure (SCD) during the first heating.

For the first heating, the common features of structural ripening at various clay content are best visualized through appropriate scaling of the data. The reduced storage modulus,

$$G'_{red} = \frac{G' - G'_{min}}{G'_{max} - G'_{min}} \quad (1)$$

allows comparison of the data. G'_{min} and G'_{max} are the lowest and highest G' values during the first temperature ramp at each respective clay content. In Fig. 2, G'_{red} data follow the same general evolution for all compositions. Nanocomposites with less than 7 wt% clay are not shown. Two distinct regimes occur due to two competing effects: (I) modulus increase due to the intercalation and exfoliation of clay which facilitates the formation of the clay–polymer network, and (II) increased chain mobility at elevated temperature which reduces the modulus. DK1/CTPB and DK4/CTPB both show the increasing trend in the regime I below 90 °C. The increased mobility in region II is more apparent for DK4/CTPB, suggesting that DK4 clay sheets exfoliate more readily and SCD establishes itself earlier. G'_{red} of DK1/CTPB levels off in regime II, suggesting that the network continues to form and, thus, structure build-up compensates the softening effect of the high temperatures; this verifies the transition temperature of 80 °C for DK1/CTPB as reported previously.[14]

Linear viscoelasticity of the stable clay dispersion (SCD) structure

In preparation of dynamic mechanical characterization of the fully developed SCD composites, we determined the critical strain amplitude γ_c at 26 °C. The strain sweep for a 9 wt% DK4/CTPB sample illustrates the typical strain dependence of G' and G'' in Fig. 3. The critical strain γ_c is experimentally chosen as the amplitude at which G' deviates more than 5% from its maximum value.[45] Increased clay content reduces the critical strain as discussed further below. Samples after strain sweeps were discarded and not subject to further rheological study, since the disordered

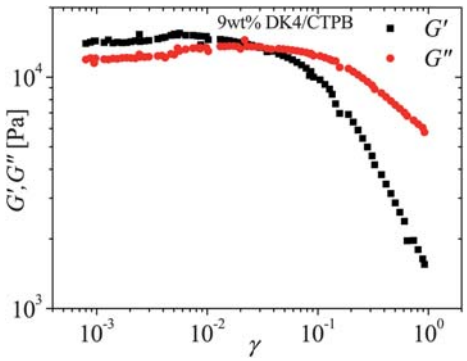

Fig. 3 Storage modulus G' and loss modulus G'' of 9 wt% DK4/CTPB SCD nanocomposites as a function of strain amplitude γ of small amplitude oscillatory shear (SAOS). The angular frequency is 10 rad s^{-1}; $T = 26$ °C.

SCD structure seems to never completely rejuvenate once destroyed by a large shear strain amplitude at the end of a strain sweep.

A sequence of many SAOS frequency sweeps between 0.01 and 100 rad s^{-1} was conducted on a single newly exfoliated SCD sample. This was necessary to avoid any subtle batch-to-batch differences due to preparation variability. Time–temperature superposition of data at 26 °C, 40 °C, 50 °C, 60 °C, 70 °C, 80 °C, 90 °C, and 100 °C resulted in the G', G'' master curves at 26 °C of Fig. 4. These master curves were generated with the aid of the IRIS rheology platform.[46]

When studying the effect of dispersed clay sheets on the steady rheological behavior, it has been argued that presenting the steady state viscosity as a function of shear stress (instead of the shear rate) is a better way to show difference in the low shear Newtonian plateau and the following shear thinning region.[32,47–49] Recently, Winter[50] proposed that the shear stress value of steady shear flow, $\tau(\dot{\gamma})$, is equivalent to the complex modulus value from SAOS, $G^*(\omega) = (G'^2 + G''^2)^{1/2}$. This gets utilized when plotting dynamic mechanical data as $\eta^*(G^*)$ (referred to as "Winter

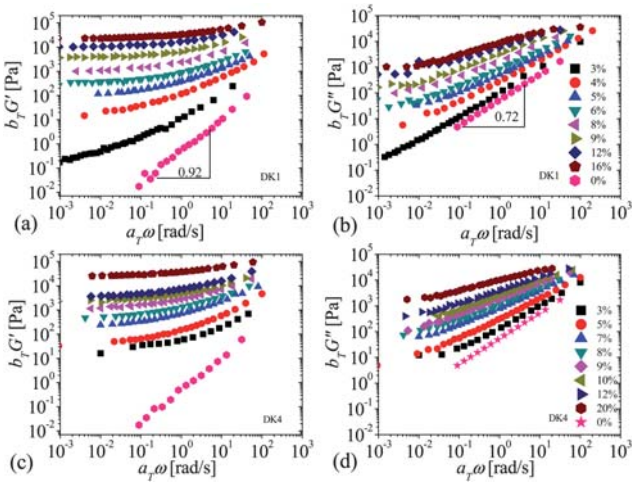

Fig. 4 Effect of clay content on fully exfoliated SCD rheology: time–temperature superposed dynamic moduli of DK1/CTPB (a and b) and DK4/CTPB (c and d). The reference temperature is 26 °C.

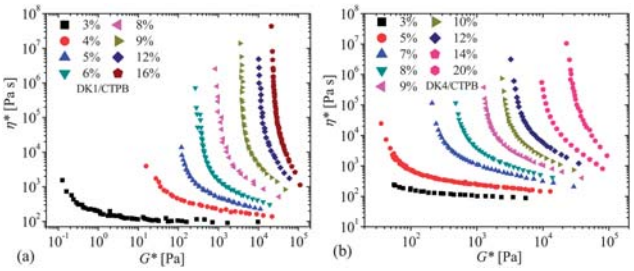

Fig. 5 Effect of clay content on fully exfoliated SCD rheology: complex viscosity η^* as function of complex modulus G^* (Winter plot): (a) DK1/CTPB and (b) DK4/CTPB. Same experimental data as in preceding figure.

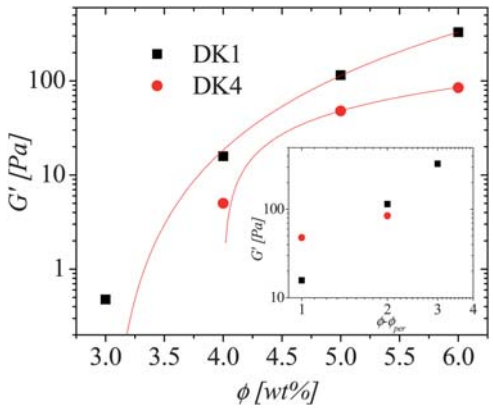

Fig. 6 Plot of the storage modulus G' measured in the low frequency regime (by extrapolation to 0 rad s^{-1}) *vs.* clay content (wt%) for DK1/CTPB and DK4/CTPB composites. Square legend: DK1/CTPB (26 °C), circle legend: DK4/CTPB (26 °C). Solid lines are the nonlinear regression according to the eqn (2). Only the data in the range of 3 wt% to 6 wt% is used for the fitting.

plot"[50]) instead of the conventional $\eta^*(\omega)$ plot. In Fig. 5, the effect of organoclay modifiers on the dynamic rheological properties becomes more apparent as the clay content increases. A yield stress is determined only when a steep upturn exists in the $\eta^*(G^*)$ curve. For both DK1/CTPB and DK4/CTPB, the yield behavior is apparent when the clay content is above 5 wt%.

4. Discussion

We start the data analysis by hypothesizing a molecular mechanism for the physical gelation. We assume that the three dimensional network is formed by tie molecules (also called "bridge molecules") that connect clay particles or, later on, clay sheets into a three dimensional network. With increasing density of tie molecules, the modulus of the gel increases. The tie molecules are assumed to connect directly onto the clay instead of onto the macro-counterions on clay surfaces. The main functions of the macro-counterions (for organically modifying the clay) are four fold:

- neutralizing the charge of the clay surface,
- sterically separating the clay sheets,
- forming a compatible blend with the matrix molecules,
- providing an environment of thermal motion that allows diffusion of matrix molecules.

The two types of counterions are very similar. The main difference between the two is the steric effect which is larger for the two-armed DK4 than for DK1. The counterion of DK4 is also slightly more compatible with the CTPB then the counterion of DK1.[13] Based on this hypothesis, we had defined the objective of this study which focuses on increased steric effects on the rheology of nanocomposite gels. The larger counterion (used for DK4) results in faster exfoliation, weaker network, higher percolation threshold, and a lower yield stress as will be discussed next.

The polymer/clay network of this study seems to behave similar as clay networks with direct particle–particle interaction. An empirical percolation model stemming from such colloidal suspension networks has been successfully employed to explain the modulus growth for polymer/clay nanocomposites with strong inter-particle interactions.[32,43,45] As the clay content is above a threshold value, single clay platelets (corresponding to exfoliation) and/or primary particles (corresponding to intercalation) can assemble into a connected network in the continuous polymer matrix with connectivity based on the high surface area and aspect ratio of dispersed clay layers. The network behaves like a weak solid and exhibits properties of a fractal structure.[35,45] A scaling relation has been proposed for the divergence of low frequency elastic modulus as

$$G' \propto (\phi - \phi_{\mathrm{Per}})^{v}, \text{ for } (\phi - \phi_{\mathrm{Per}}) > 0, \qquad (2)$$

where v is the power-law exponent; ϕ is the clay content, and ϕ_{Per} is the percolation threshold at which the connection structure spanning the whole sample is first time formed. In this paper ϕ is measured by the weight fraction instead of the usual volume fraction due to the lack of accurate clay density data. $(\phi - \phi_{\mathrm{Per}})$ marks the distance beyond the percolation threshold. Fig. 6 shows the evaluation of the percolation model for the low clay content nanocomposites. The storage moduli of both, DK1/CTPB and DK4/CTPB, fit the percolation model quite closely. As a result of the fitting, the determined percolation threshold ϕ_{Per} is about 3 wt% (~1.6 vol%) and 4 wt% (~2.1 vol%) with power law exponents 2.63 and 0.83 for DK1/CTPB and DK4/CTPB, respectively.

Vermant *et al.*[32] related the percolation threshold to the dispersion state of clay in a polymer matrix (non-sticky). Higher exfoliation degree meant a more open fractal structure, resulting in a lower percolation threshold. This correlation does not apply here since both DK1/CTPB and DK4/CTPB are highly exfoliated in the SCD state.[13] Cassagnau[43] pointed out that the percolation threshold may depend on the type of surfactant used to modify clay organophilic capability and/or on the compatibilizers used to enhance clay affinity with the polymer matrix. Beyond the threshold, soft solid behavior governs with a pronounced increase of the dynamic moduli whose origin is still subject of debate,[51–53] however, polymer–particle interactions have been identified as the most important factor.[13,14,43,54,55]

The pioneering theoretical work of Balazs *et al.*[41,56–58] and of Farmer[59] proposes that end-functional groups of telechelic polymer chains can serve as surface-active or 'sticker' sites in which oxygen strongly attracts to hydroxyls of clay sheets, provided that its chain ends get sufficiently close to a clay surface.

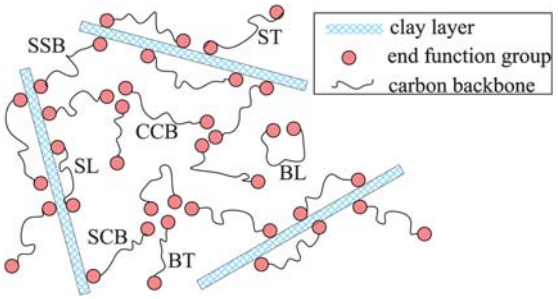

Fig. 7 Schematic conformations of end functional polymer chains in dispersed clay sheets according to Malvaldi *et al.*[60] classification. Seven possible chain conformations are: BT = bulk tail (including free open chains), BL = bulk loop, ST = surface tail, SL = surface loop, CCB = cluster–cluster bridge, SSB = surface–surface bridge and SCB = surface–cluster bridge. Each chain can be classified to one or multiple conformations listed above, but not all chains are labeled here to prevent crowding. The counterions are not shown.

Malvaldi *et al.*[60] discussed seven possible states of telechelic polymer chains in the confined space between clay sheets for molecular dynamic simulation purpose (referred to as Malvaldi *et al.* classification), see Fig. 7. In general, polymer chain end group might aggregate in bulk (end linking) or adsorb on the clay surface. The physical network of this study seems to get its connectivity from surface–surface bridge (SSB) chains while end linking (CCB) and surface–cluster bridges (weak 'indirect' SCB cross-links) seem to be negligible. Surface loops (SLs) do not contribute to the connection but contribute to the steric separation of clay sheets. The overall strength of the particle–polymer network is determined by a subtle balance between steric separation effects and particle–particle gluing by bridge molecules.

Two long hydrophilic tails (D18A) offer a better compatibility with CTPB when compared with one long tail (C18A). This has been validated *via* the turbidity comparison between C18A/CTPB mixtures and D18A/CTPB mixtures by Zhu *et al.*[13] However, the two alkyl tails of D18A which will hinder the end-functionalized groups of CTPB contacting with the clay surface. The chance of CTPB chains taking SSB and SCB conformations at DK4 surfaces is lower than that at DK1 surfaces. A weak polymer–particle network results in a higher percolation threshold. Here the explanation is only qualitative, further thermodynamic analysis of impact of organic modifier on the distribution of chain formations lies beyond the scope of the present work.

Master curves of the storage and loss moduli (G', G'') for CTPB nanocomposites of various DK1/DK4 clay contents and pure CTPB are compared in **Fig. 4**. The dispersed clay sheets affect the linear viscoelastic response of nanocomposites in two aspects: dynamic moduli increasing in the whole frequency range and the solid-like behavior at low frequency. Pure CTPB is fully relaxed and exhibits characteristic liquid-like terminal behavior, showing the power-law dependence on frequency, and the power exponents are noted on plots. As the clay content is raised above the percolation threshold, there is an apparent plateau in G' at low frequency range which is typical for solid behavior. This suggests the emergence of a network structure consisting of particle–particle attraction and/or particle–polymer interaction. Dynamic moduli of clay/CTPB nanocomposites are two or three orders of magnitude higher than for pure CTPB, depending on the clay content. For nanocomposites that form a network structure due to direct particle–particle interaction, it has been observed that the difference between dynamic moduli of nanocomposites and pure polymer vanishes as frequency increases, since the polymer matrix contributes more strongly to the linear viscoelastic behavior at high frequencies.[32,37,61] The fact that differences between dynamic moduli of our nanocomposites and those of pure CTPB remain at high frequencies suggests a strong or dominant particle–polymer interaction.

The origin of the solid behavior in nanocomposites is still controversial. In addition to the widely accepted fractal network of dispersed clay sheets,[32,34,35,62] solid properties have been attributed to the confined polymer chains between silicate layers.[45,63–66] Galgali *et al.*[67] argued that the solid rheological response of the molten nanocomposites originates from large frictional interactions between dispersed silicate layers. The surface loops (SLs) shown in **Fig. 7** do not contribute to the connection of clay sheets, as discussed in the percolation threshold. However, they might facilitate the diffusion of clay sheets. The higher ratio of SLs in the DK4/CTPB will weaken the strength of the network which requires particle–polymer connectivity.

Shih and co-workers[45] studied space-filling colloidal networks and proposed a scaling law (referred to as the Shih model) which is based on the concept of a particle network of fractal flocs that aggregate. Vermant *et al.* adapted the Shih model to clay nanocomposites to predict viscoelastic properties with increased clay fraction:[32]

$$G'_{\mathrm{P}} \propto \phi^{(3+x)/(3-d_{\mathrm{f}})}, \text{ for } \phi \gg \phi_{\mathrm{Per}}, \tag{3}$$

where G'_{P} is the clay/CTPB plateau storage modulus at low frequencies, or the equilibrium modulus $G_0 = \lim_{\omega \to 0} G'(\omega)$, d_{f} is the fractal dimension of the aggregate network, and x is an exponent which depends on the number of particles per aggregate. Similarly the critical strain is expressed as

$$\gamma_{\mathrm{c}} \propto \phi^{-(1+x)/(3-d_{\mathrm{f}})} \tag{4}$$

Only data at the clay content far above the percolation threshold are used when analyzing the linear viscoelastic properties of clay/CTPB nanocomposites according to the Shih/Vermant model. The equilibrium modulus G_0 is taken from the storage modulus G' plateau as shown in Fig. 4(a) and (b), as limiting values of G' at the lowest accessible frequencies. The data and nonlinear regression of G_0 and γ_{c} are shown in Fig. 8(a) and (b). In the log–log scale, the points of G_0 of DK1/CTPB and DK4/CTPB both render straight lines as predicted by the power-law in eqn (3). γ_{c} shows the proposed linear behavior for DK4/CTPB, but not for DK1/CTPB where it is almost independent of the clay content. Simultaneously fitting of eqn (3) and (4) to the data results in values of x and d_{f}.[32,68] x and d_{f} for DK4/CTPB were found as −0.169 and 2.391, respectively. This is in contradiction to assumptions in the Shih/Vermant model which requires that x values should always be positive. The failure of linear regression of γ_{c} of DK1/CTPB and a negative value of the solved x for DK4/CTPB suggest that neither of two nanocomposites fits the Shih/Vermant model. This should not surprise since

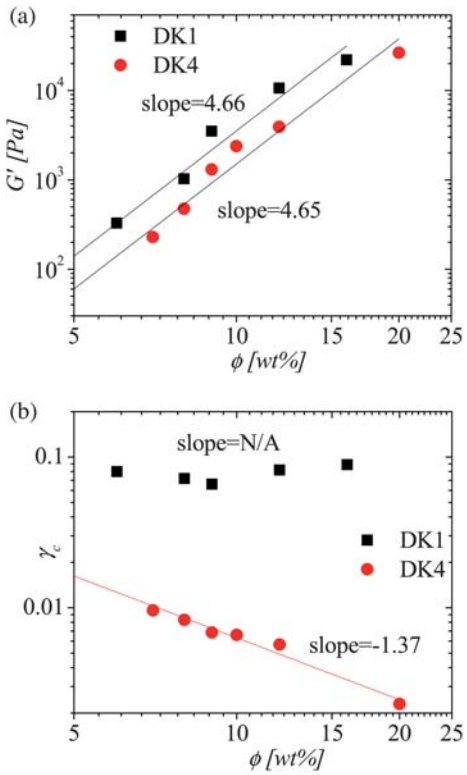

Fig. 8 (a) The equilibrium modulus G_0 and (b) the critical strain γ_c of DK1/CTPB and DK4/CTPB nanocomposites as a function of the clay content (far above the percolation threshold value). The solid lines are a linear regression (in a double-logarithmic scale) according to eqn (3) and (4). The critical strain γ_c of DK1/CTPB fails in the nonlinear regression. Only the points above 6 wt% are used for the fitting.

particle–polymer interaction is not taken into account in the Shih/Vermant model, in which the elastic backbone of the connected network is approximated to be a linear chain of springs. This assumption does not apply to DK1/CTPB and DK4/CTPB nanocomposites, for the bridge molecules connecting clay sheets play an important role in the network formation.

For comparison and a check for the need of the end functionalization, we used PB without end group in stand of CTPB. The corresponding rheological experiments showed that the polymer and clay interaction is very weak.[11–13]

5. Conclusions

A final stable clay dispersion was achieved by heating the nanocomposites to a temperature above 100 °C, but without applying flow. Solid behavior was observed above a fairly low threshold concentration of clay. The existing network structure causes the storage modulus to plateau in the low frequency range and to shear thin at large shear strain. The vast difference between the high frequency dynamic moduli between Clay/CTPB nanocomposites and those of pure CTPB confirms the strong interaction between the polymer and the clay surfaces. The interaction between the organically modified clay and end-functionalized molecules essentially contributes to the network formation.

Under comparable conditions, DK4 was found to exfoliate faster in CTPB than DK1, as shown in **Fig. 2**. This is attributed to the wider spacing between clay sheets when applying the large counterion of DK4. The high compatibility of the two-tailed counterion with CTPB is also assumed to contribute to this accelerated ripening of the structure. The wider spacing due to the larger counterion, however, weakens the network connectivity. When comparing to DK1/CTPB, DK4/CTPB requires a higher clay concentration to percolate. Also, DK4/CTPB forms the gel with the lower modulus. These network properties are attributed to a dominant steric effect of the counterion on the clay surface. The two-armed counterions in DK4 hinder CTPB from attaching to the clay surface, which results in a weaker polymer–clay interaction and a lower concentration of bridge molecules.

Acknowledgements

HHW acknowledges the support of NSF CBET 0651888 and CBET 0943474. This work was supported by National Natural Science Foundation of China (Grants 20904020), the China Postdoctoral Science Foundation and Jiangsu Planned Projects for Postdoctoral Research Funds.

References

1 S. D. Burnside and E. P. Giannelis, *J. Polym. Sci., Part B: Polym. Phys.*, 2000, **38**, 1595–1604.
2 J. Carretero-Gonzalez, H. Retsos, R. Verdejo, S. Toki, B. S. Hsiao, E. P. Giannelis and M. A. Lopez-Manchado, *Macromolecules*, 2008, **41**, 6763–6772.
3 J. W. Gilman, C. L. Jackson, A. B. Morgan, R. Harris, E. Manias, E. P. Giannelis, M. Wuthenow, D. Hilton and S. H. Phillips, *Chem. Mater.*, 2000, **12**, 1866–1873.
4 P. C. LeBaron, Z. Wang and T. J. Pinnavaia, *Appl. Clay Sci.*, 1999, **15**, 11–29.
5 D. Shah, P. Maiti, D. D. Jiang, C. A. Batt and E. P. Giannelis, *Adv. Mater.*, 2005, **17**, 525–530.
6 R. A. Vaia, G. Price, P. N. Ruth, H. T. Nguyen and J. Lichtenhan, *Appl. Clay Sci.*, 1999, **15**, 67–92.
7 W. Xu, S. Raychowdhury, D. D. Jiang, H. Retsos and E. P. Giannelis, *Small*, 2008, **4**, 662–669.
8 M. Alexandre and P. Dubois, *Mater. Sci. Eng., R*, 2000, **28**, 1–63.
9 E. P. Giannelis, *NATO Advanced Research Workshop on Nanostructured Films and Coatings*, Santorini, Greece, 1999.
10 P. B. Messersmith and E. P. Giannelis, *J. Polym. Sci., Part A: Polym. Chem.*, 1995, **33**, 1047–1057.
11 T. H. Chen, J. J. Zhu, B. H. Li, S. Y. Guo, Z. Y. Yuan, P. C. Sun, D. T. Ding and A. C. Shi, *Macromolecules*, 2005, **38**, 4030–4033.
12 X. L. Wang, Y. Gao, K. M. Mao, G. Xue, T. H. Chen, J. J. Zhu, B. H. Li, P. C. Sun, Q. H. Jin, D. T. Ding and A. C. Shi, *Macromolecules*, 2006, **39**, 6653–6660.
13 J. J. Zhu, X. L. Wang, F. F. Tao, G. Xue, T. H. Chen, P. C. Sun, Q. H. Jin and D. T. Ding, *Polymer*, 2007, **48**, 7590–7597.
14 X. L. Wang, F. F. Tao, G. Xue, J. J. Zhu, T. H. Chen, P. C. Sun, H. H. Winter and A. C. Shi, *Macromol. Mater. Eng.*, 2009, **294**, 190–195.
15 X. L. Wang, P. C. Sun, G. Xue and H. H. Winter, *Macromolecules*, 2010, **43**, 1901–1906.
16 H. H. Winter, X. L. Wang, G. Xue and P. C. Sun, *Polym. Prepr. (Am. Chem. Soc., Div. Polym. Chem.)*, 2009, **50**, 80–81.
17 S. A. Monemian, V. Goodarzi, P. Zahedi and M. T. Angaji, *Adv. Polym. Technol.*, 2007, **26**, 247–257.
18 R. R. Qi, X. Jin, J. H. Nie, W. Yu and C. X. Zhou, *J. Appl. Polym. Sci.*, 2005, **97**, 201–207.
19 M. W. Weimer, H. Chen, E. P. Giannelis and D. Y. Sogah, *J. Am. Chem. Soc.*, 1999, **121**, 1615–1616.

20 A. Usuki, Y. Kojima, M. Kawasumi, A. Okada, Y. Fukushima, T. Kurauchi and O. Kamigaito, *J. Mater. Res.*, 1993, **8**, 1179–1184.
21 D. C. Lee and L. W. Jang, *J. Appl. Polym. Sci.*, 1996, **61**, 1117–1122.
22 D. Donescu and M. C. Corobea, *J. Dispersion Sci. Technol.*, 2007, **28**, 671–679.
23 C. O. Oriakhi, I. V. Farr and M. M. Lerner, *Clays Clay Miner.*, 1997, **45**, 194–202.
24 K. A. Carrado and L. Q. Xu, *Chem. Mater.*, 1998, **10**, 1440–1445.
25 L. Q. Xu and K. A. Carrado, *Abstr. Pap. Am. Chem. Soc.*, 1999, **218**, 743.
26 L. M. Liu, Z. N. Qi and X. G. Zhu, *J. Appl. Polym. Sci.*, 1999, **71**, 1133–1138.
27 T. McNally, W. R. Murphy, C. Y. Lew, R. J. Turner and G. P. Brennan, *Polymer*, 2003, **44**, 2761–2772.
28 W. Awad, A. Esawi and A. Ramadan, *2nd Multifunctional Nanocomposites and Nanomaterials International Conference and Exhibition*, Sharm El Sheikh, Egypt, 2008.
29 D. Kim, J. S. Lee, C. F. Barry and J. L. Mead, *J. Appl. Polym. Sci.*, 2008, **109**, 2924–2934.
30 D. W. Litchfield and D. G. Baird, *Polymer*, 2008, **49**, 5027–5036.
31 T. D. Fornes, P. J. Yoon, H. Keskkula and D. R. Paul, *Polymer*, 2001, **42**, 9929–9940.
32 J. Vermant, S. Ceccia, M. K. Dolgovskij, P. L. Maffettone and C. W. Macosko, *J. Rheol.*, 2007, **51**, 429–450.
33 K. Wang, S. Liang, J. N. Deng, H. Yang, Q. Zhang, Q. Fu, X. Dong, D. J. Wang and C. C. Han, *Polymer*, 2006, **47**, 7131–7144.
34 J. X. Ren, A. S. Silva and R. Krishnamoorti, *Macromolecules*, 2000, **33**, 3739–3746.
35 M. J. Solomon, A. S. Almusallam, K. F. Seefeldt, A. Somwangthanaroj and P. Varadan, *Macromolecules*, 2001, **34**, 1864–1872.
36 L. Solar, A. Nohales, R. Munoz-Espi, D. Lopez and C. M. Gomez, *J. Polym. Sci., Part B: Polym. Phys.*, 2008, **46**, 1837–1844.
37 E. Nazockdast, H. Nazockdast and F. Goharpey, *Polym. Eng. Sci.*, 2008, **48**, 1240–1249.
38 J. M. Kropka, K. W. Putz, V. Pryamitsyn, V. Ganesan and P. F. Green, *Macromolecules*, 2007, **40**, 5424–5432.
39 H. Tokui and K. Yamazaki, *Bull. Chem. Soc. Jpn.*, 1966, **39**, 2290–2294.
40 S. S. Ray and M. Okamoto, *Prog. Polym. Sci.*, 2003, **28**, 1539–1641.
41 A. C. Balazs, C. Singh and E. Zhulina, *Macromolecules*, 1998, **31**, 8370–8381.
42 S. Pavlidou and C. D. Papaspyrides, *Prog. Polym. Sci.*, 2008, **33**, 1119–1198.
43 P. Cassagnau, *Polymer*, 2008, **49**, 2183–2196.
44 E. P. Giannelis, R. Krishnamoorti and E. Manias, *Adv. Polym. Sci*, 1999, **138**, 107–147.
45 W. H. Shih, W. Y. Shih, S. I. Kim, J. Liu and I. A. Aksay, *Phys. Rev. A*, 1990, **42**, 4772–4779.
46 H. H. Winter and M. Mours, *Rheol. Acta*, 2006, **45**, 331–338.
47 T. Kataoka, T. Kitano, M. Sasahara and K. Nishijima, *Rheol. Acta*, 1978, **17**, 149–155.
48 P. Moldenaers, H. Yanase and J. Mewis, *ACS Symp. Ser.*, 1990, **435**, 370–380.
49 N. Ohl and W. Gleissle, *J. Rheol.*, 1993, **37**, 381–406.
50 H. H. Winter, *Rheol. Acta*, 2009, **48**, 241–243.
51 G. Heinrich and M. Kluppel, in *Filled Elastomers Drug Delivery Systems*, Springer-Verlag Berlin, Berlin, 2002, vol. 160, pp. 1–44.
52 Y. H. Hyun, S. T. Lim, H. J. Choi and M. S. Jhon, *Macromolecules*, 2001, **34**, 8084–8093.
53 A. I. Medalia, *Rubber Chem. Technol.*, 1978, **51**, 437–523.
54 P. G. Maier and D. Goritz, *Kautsch. Gummi Kunstst.*, 1996, **49**, 18–21.
55 S. S. Sternstein and A. J. Zhu, *Macromolecules*, 2002, **35**, 7262–7273.
56 E. Zhulina, C. Singh and A. C. Balazs, *Langmuir*, 1999, **15**, 3935–3943.
57 V. V. Ginzburg and A. C. Balazs, *Adv. Mater.*, 2000, **12**, 1805–1809.
58 Y. Lyatskaya and A. C. Balazs, *Macromolecules*, 1998, **31**, 6676–6680.
59 A. Sinsawat, K. L. Anderson, R. A. Vaia and B. L. Farmer, *J. Polym. Sci., Part B: Polym. Phys.*, 2003, **41**, 3272–3284.
60 M. Malvaldi, G. Allegra, F. Ciardelli and G. Raos, *J. Phys. Chem. B*, 2005, **109**, 18117–18126.
61 S. Y. Gu, J. Ren and B. Dong, *J. Polym. Sci., Part B: Polym. Phys.*, 2007, **45**, 3189–3196.
62 R. Krishnamoorti and K. Yurekli, *Curr. Opin. Colloid Interface Sci.*, 2001, **6**, 464–470.
63 G. Luengo, F. J. Schmitt, R. Hill and J. Israelachvili, *Macromolecules*, 1997, **30**, 2482–2494.
64 E. Manias, V. Kuppa, D. K. Yang and D. B. Zax, *2nd International TRI/Princeton Workshop on Characterization of Porous Materials*, Princeton, New Jersey, 2000.
65 A. Subbotin, A. Semenov and M. Doi, *Phys. Rev. E: Stat. Phys., Plasmas, Fluids, Relat. Interdiscip. Top.*, 1997, **56**, 623–630.
66 D. B. Zax, D. K. Yang, R. A. Santos, H. Hegemann, E. P. Giannelis and E. Manias, *J. Chem. Phys.*, 2000, **112**, 2945–2951.
67 G. Galgali, C. Ramesh and A. Lele, *Macromolecules*, 2001, **34**, 852–858.
68 A. Durmus, A. Kasgoz and C. W. Macosko, *Polymer*, 2007, **48**, 4492–4502.

